MolecularMedicine

Humanin Derivatives Inhibit Necrotic Cell Death in Neurons

Aviv Cohen,[1] Jenny Lerner-Yardeni,[1] David Meridor,[1] Roni Kasher,[2] Ilana Nathan,[3,4] and Abraham H Parola[1]*

[1]Department of Chemistry, The Faculty of Natural Sciences, Ben-Gurion University of the Negev, Be'er-Sheva, Israel; [2]Department of Desalination and Water Treatment, Zuckerberg Institute for Water Research, The Blaustein Institutes for Desert Research, Ben-Gurion University of the Negev, Sede Boqer Campus, Midreshet Sede Boqer, Israel; [3]Department of Clinical Biochemistry and Pharmacology, The Faculty of Health Sciences, Ben-Gurion University of the Negev, Be'er-Sheva, Israel; [4]Institute of Hematology, Soroka University Medical Center, Be'er-Sheva, Israel; and *current affiliation: Faculty of Arts and Sciences, NYU Shanghai, Shanghai, People's Republic of China

Humanin and its derivatives are peptides known for their protective antiapoptotic effects against Alzheimer's disease. Herein, we identify a novel function of the humanin-derivative AGA(C8R)-HNG17 (namely, protection against cellular necrosis). Necrosis is one of the main modes of cell death, which was until recently considered an unmoderated process. However, recent findings suggest the opposite. We have found that AGA(C8R)-HNG17 confers protection against necrosis in the neuronal cell lines PC-12 and NSC-34, where necrosis is induced in a glucose-free medium by either chemohypoxia or by a shift from apoptosis to necrosis. Our studies in traumatic brain injury models in mice, where necrosis is the main mode of neuronal cell death, have shown that AGA(C8R)-HNG17 has a protective effect. This result is demonstrated by a decrease in a neuronal severity score and by a reduction in brain edema, as measured by magnetic resonance imaging (MRI). An insight into the peptide's antinecrotic mechanism was attained through measurements of cellular ATP levels in PC-12 cells under necrotic conditions, showing that the peptide mitigates a necrosis-associated decrease in ATP levels. Further, we demonstrate the peptide's direct enhancement of the activity of ATP synthase activity, isolated from rat-liver mitochondria, suggesting that AGA(C8R)-HNG17 targets the mitochondria and regulates cellular ATP levels. Thus, AGA(C8R)-HNG17 has potential use for the development of drug therapies for necrosis-related diseases, for example, traumatic brain injury, stroke, myocardial infarction, and other conditions for which no efficient drug-based treatment is currently available. Finally, this study provides new insight into the mechanisms underlying the antinecrotic mode of action of AGA(C8R)-HNG17.

Online address: http://www.molmed.org
doi: 10.2119/molmed.2015.00073

INTRODUCTION

Necrosis refers to the process of cell death accompanied by the rapid efflux of cell constituents into the extracellular space, which may induce a marked inflammatory response (1,2). The membrane damage is induced by morphological events that cause an increase in cell membrane permeability, with debilitating effects. During necrosis, the cells first swell and then the plasma membranes collapse, rapidly leading to cellular lysis. Necrosis does not exhibit the activation of caspases or oligonucleosomal DNA fragmentation, which are the biochemical hallmarks of apoptosis; however, erratic proteolysis and random degradation of DNA do take place. Necrosis was formerly considered to be a passive and unregulated process (3,4). However, recent findings have identified associated biochemical events, such as signal transduction and the oxidation of specific phospholipids (5,6), indicating that necrosis is a controlled process. An example of necrosis is ischemia, which leads to the dramatic depletion of oxygen, glucose, and other trophic factors, provoking massive necrotic death.

Humanin is a 24–amino acid mitochondrial-derived peptide (MAPRGFSCLLLLTSEIDLPVKRRA) that was discovered in 2001 by Hashimoto *et al.* (7–9) by using a cDNA library constructed from brain tissue recovered from a deceased patient with Alz-

Address correspondence to *Roni Kasher, Department of Desalination and Water Treatment, Zuckerberg Institute for Water Research, The Blaustein Institutes for Desert Research, Ben-Gurion University of the Negev. Midreshet Ben-Gurion 8499000, Israel. Phone: +972-8-6563531; Fax: +972-8-6596889; E-mail: kahser@bgu.ac.il; or Ilana Nathan, Department of Clinical Biochemistry and Pharmacology, the Faculty of Health Sciences, Ben-Gurion University of the Negev. P.O Box 653 Be'er-Sheva 8410501, Israel. Phone: +972-8-6400263; Fax: 972-8-6244058; E-mail: nathan@bgu.ac.il; or Abraham H Parola, Department of Chemistry, the Faculty of Natural Sciences, Ben-Gurion University of the Negev. P.O Box 653 Be'er-Sheva 8410501, Israel. Phone: +972-52-8795945; Fax: +972-8-647294; E-mail: aparola@bgu.ac.il; ap137@nyu.edu.*
Submitted March 25, 2015; Accepted for publication June 1, 2015; Published Online (www.molmed.org) June 4, 2015.

heimer's disease (AD). Humanin expression in humans has been shown to decrease with age, which suggests a possible causal relationship between decreased humanin and the onset of "old age" diseases such as AD and type 2 diabetes (10). Humanin can suppress apoptotic cell death stemming from various insults, such as AD-related amyloid β (Aβ), serum deprivation and ischemia reperfusion (11–13). Design of peptides with higher activity was performed by systematic screening of peptides based on the amino acid sequence of humanin, which resulted in several derivatives with higher antiapoptotic activity (9,14,15).

Several receptors, such as formyl peptide receptors 1 and 2 and the interleukin-6 receptors family including ciliary neurotrophic factor receptor subunit alpha (CNTFRα), interleukin 27 receptor, alpha subunit (WSX1) and glycoprotein 130 (GP130), are thought to bind humanin (16–20). An intracellular antiapoptotic mechanism has been demonstrated, revealing the capacity of humanin to bind the Bcl-2-associated X protein (BAX) protein family (21–24). It was also found that humanin can increase cellular ATP levels (25). Serum-deprived lymphocytes with low levels of ATP regain their ATP with the addition of humanin; this also occurs in non–serum-deprived cells. We thus hypothesize that the effect of increasing ATP levels related to humanin may lead to additional activity inhibiting necrotic cell death, in which depletion of ATP plays a major role.

Here, we report novel *in vitro* and *in vivo* antinecrotic activities of humanin derivatives; among them, the peptide AGA(C8R)-HNG17 showed the highest potency. AGA(C8R)-HNG17 showed a protective effect in traumatic brain injury (TBI) in mice, where necrosis is the main mode of neuronal cell death. AGA(C8R)-HNG17 was found to antagonize the decrease in ATP levels associated with necrosis in PC-12 cells. The peptide directly enhanced the activity of the ATP synthase complex isolated from rat liver mitochondria, suggesting that this humanin derivative targets the mitochondria, regulating cellular ATP levels. To the best of our knowledge, this is the first report of the antinecrotic effects of humanin derivatives.

MATERIALS AND METHODS

Materials for Peptide Synthesis

The following protected (L)-amino acids were used for peptide synthesis: fluorenylmethoxycarbonyl (Fmoc)-Ala-OH, Fmoc-Arg(Pbf)-OH, Fmoc-Asn(Trt)-OH, Fmoc-Asp(OtBu)-OH, Fmoc-Cys(Trt)-OH, Fmoc-Gln(Trt)-OH, Fmoc-Glu(OtBu)-OH, Fmoc-Gly-OH, Fmoc-Ile-OH, Fmoc-Leu-OH, Fmoc-Lys(Boc)-OH, Fmoc-Met-OH, Boc-Met-OH, Fmoc-Phe-OH, Fmoc-Pro-OH, Boc-Pro-OH, Fmoc-Ser(tBu)-OH, Fmoc-Thr(tBu)-OH, Fmoc-Trp(Boc)-OH, Fmoc-Tyr(tBu)-OH and Fmoc-Val-OH, and pseudoproline dipeptides Fmoc-Leu-Thr ($\Psi^{Me,Me}$pro)-OH and Fmoc-Ala-Ser($\Psi^{Me,Me}$Pro)-OH. These amino acids were Advanced ChemTech, Iris Biotech GmbH, Novabiochem and Chem-Impex International products. The resins 2-Cl-Trt resin (100–200 mesh) and Fmoc-Ala-Wang resin (100–200 mesh, 0.8 mmol/g) were used for peptide synthesis and were Novabiochem products. *N*-Methyl-2-pyrrolidone, methylene chloride, dimethylformamide (DMF) (peptide synthesis grade), acetonitrile (high-performance liquid chromatography [HPLC] ultragrade) and H_2O (HPLC ultragrade) were J.T. Baker products. *O*-Benzotriazole-*N*,*N*,*N*′,*N*′-tetramethyl-uronium-hexafluorophosphate (HBTU) was a Chem-Impex International product. Piperidine, *N*,*N*-diisopropylethylamine (DIEA), trifluoroacetic acid (TFA) and *tert*-butylmethyl ether were Bio-Lab products. 1,2-Ethanedithiol and triisopropylsilane were Sigma products.

Material for Cell Viability Assays

Dulbecco modified Eagle medium (DMEM) and RPMI-1640 medium were Gibco products; glucose-free RPMI-1640 medium, fetal calf serum (FCS), penicillin/streptomycin solution (penicillin 10,000 U/mL; streptomycin 10 mg/mL), 200 mmol/L L-glutamine solution and phosphate-buffered saline (PBS) were Biological Industries products. The CytoTox 96® Non-Radioactive Cytotoxicity Assay Kit was a Promega product. Trypan blue, acridine orange (AO), ethidium bromide (EtBr), potassium cyanide (KCN), staurosporine (STS) and oligomycin-A were Sigma products. The ATP assay system bioluminescence detection kit was a Calbiochem product. An ATP synthase Enzyme Activity Microplate Assay Kit was an Abcam product.

Peptide Synthesis

Humanin and its derivatives were synthesized by using standard protocols for solid-phase peptide synthesis, which relies on Fmoc chemistry. Amino acid coupling was performed with five equivalents (eq) of N-protected amino acid, 5 eq HBTU and 10 eq DIEA relative to the resin. Fmoc deprotection was performed with 20% piperidine in DMF solution (for 5 min and again for 25 min). The first 10 amino acids of each synthesis were coupled for 45 min, and the following amino acids were doubly coupled (46 min each coupling). Synthesis was performed by using a CS336S automated peptide synthesizer (CS Bio). All HN derivatives except AGA(C8R)-HNG17 were synthesized by using Fmoc-Ala-Wang resin; AGA(C8R)-HNG17 was synthesized by using 2-Cl-Trt resin.

The peptides were purified with a preparative reverse-phase (RP)-HPLC apparatus equipped with Waters 600 Semi-Prep HPLC controller and quaternary pump and with a Waters 2487 dual λ absorbance detector equipped with a manual injector with a loop volume of 5 mL (Rheodyne) by using a C18 column (Phenomenex "Jupiter": 250 × 21.20 mm with 10-μm pore size). The preparative method involved a flow rate of 12 mL/min with a gradient of 15% B to 70% B in 50 min (eluents as in analytical HPLC). Peptides were purified to >95% purity.

The peptide purities were evaluated with an analytical RP-HPLC apparatus equipped with a Surveyor UV/Vis De-

tector, Surveyor Auto-sampler Plus, and Surveyor LC Pump Plus (Thermo Fisher Scientific). The C18 column used was a Phenomenex "Gemini": 250 × 4.60 mm with 5-μm pore sizes. The analytical method involved a flow rate of 1 mL/min with a gradient of 15% B to 70% B in 40 min (eluent A: 0.1% TFA in double-distilled water; eluent B: 75% acetonitrile [ACN], 25% double-distilled water and 0.085% TFA). Peptide identification was performed with a Reflex-IV Matrix-Assisted Laser Desorption/Ionization Time of Flight Mass Spectroscopy apparatus (Brucker). The samples were prepared with α-cyano-4-hydroxycinnamic acid or dihydroxybenzoic acid matrices (see Supplementary Table S1).

All peptides were dissolved in PBS for *in vivo* and *in vitro* activity assays and kept at –80°C in aliquots.

Cell Lines

The rat pheochromocytoma PC-12 cell line was maintained in DMEM and supplemented with 7.5% heat-inactivated FCS, 15% heat-inactivated horse serum, 100 U/mL penicillin, 100 μg/mL streptomycin and 2 mmol/L L-glutamine. The cells were cultured in 75-cm^2 flasks and grown at 37°C under an atmosphere of 5% CO_2 and 95% air. The cells were subcultured every 3–4 d. The NSC-34 cell line was grown in DMEM supplemented with 10% FCS, 100 U/mL penicillin, 100 μg/mL streptomycin and 2 mmol/L L-glutamine. The cells were cultured in 75-cm^2 flasks and grown under an atmosphere of 5% CO_2 and 95% air. Cells were subcultivated every 3–4 d by trypsinization.

To measure cell viability and determine the mode of cell death, cells in the logarithmic phase were seeded at a concentration of 2×10^5 cells/mL in 24- or 96-well plates coated with collagen and preincubated under an atmosphere of 5% CO_2 and 95% air for 24 h before treatment.

KCN-Induced Necrosis

Cyanide is an inhibitor of cytochrome-c oxidase (complex IV) and thus blocks ATP synthesis in the mitochondria; under glucose-free conditions, apoptotic cell death is negligible and cell death occurs via necrosis because of lack of ATP. Chemohypoxia was induced in NSC-34, and PC-12 cells in the logarithmic phase were seeded in complete DMEM overnight at a concentration of 2×10^5 cells/well. The cells were washed once and maintained in glucose-free RPMI-1640 medium supplemented with 2 mmol/L pyruvate and 10% dialyzed FCS for 1 h. Different concentrations of humanin derivatives dissolved in PBS (or PBS as a vehicle) were added 30 min before treatment with or without different concentrations of KCN. Cell death assessment was performed 5 h after addition of KCN.

Staurosporine/Oligomycin-A–Induced Necrosis

Treatment with a low concentration of oligomycin-A together with STS results in a shift in the cell death mechanism from apoptosis to necrosis. This happens because oligomycin-A is an inhibitor of F_0F_1-ATPase and thus blocks ATP synthesis; on addition of STS, the cell death mechanism shifts from apoptosis to necrosis. PC-12 cells in the logarithmic phase were seeded in complete DMEM overnight at a concentration of 2×10^5 cells/well in 24-well plates (Bio-Fil). The cells were washed once with PBS and maintained in glucose-free RPMI-1640 medium, supplemented with 2 mmol/L pyruvate and 10% dialyzed FCS, for 1 h before treatment with humanin derivatives. Different concentrations of humanin derivatives dissolved in PBS, or vehicle, were added 30 min before treatment. The PC-12 cells were incubated with and without 1 μmol/L oligomycin for 30 min and then treated with or without 1.25 μmol/L STS. Cell death assessment was done 5 h after treatment with staurousporine (26,27).

Trypan Blue Exclusion Assay

To directly assess the number of live and dead cells after treatment, PC-12 cells (2×10^5 cells/mL) were seeded in 24-well plates and treated 24 h after seeding. At the end of each experiment, the cells were trypsinized and pelleted together with those cells in the culture supernatant. Trypan blue (Sigma), which is excluded from live cells and stains only dead cells, was dissolved in saline (0.9% sodium chloride) to a concentration of 2 mg/mL. A volume of 25 μL of cell in suspension was added to 225 μL Trypan blue solution with 0.2% saline. After staining with Trypan blue solution, the viable (unstained) cells were counted in a hemocytometer chamber (28,29).

Lactate Dehydrogenase Release Assay

Necrotic cell death was measured in 96-well plates by using the CytoTox 96 nonradioactive cytotoxicity assay kit (Promega) to measure cell death by quantitating the release of lactate dehydrogenase, a stable cytosolic enzyme, from lysed cells. Cells were seeded in 96-well plates and treated 24 h after seeding. At the end of each experiment, conducted for the indicated time period, the cells were centrifuged at 240*g* for 10 min at room temperature. The supernatant was collected and 50-μL aliquots were taken for the lactate dehydrogenase release assay. The lactate dehydrogenase content of cells lysed in 0.1% Triton X-100 for 10–15 min served as a measure of the total lactate dehydrogenase content. The lactate dehydrogenase released during treatment was used, after blank subtraction, as a measure of necrotic cell death, expressed as a percentage of the total lactate dehydrogenase activity. Sample absorbance at 490 nm was measured with an enzyme-linked immunosorbent assay (ELISA) reader 30 min after the addition of the lactate dehydrogenase reaction solution.

Morphological Quantification of Necrosis and Apoptosis with Ethidium Bromide and Acridine Orange

To differentiate between apoptotic and necrotic cell death, cells were stained with AO and EtBr and examined under a fluorescence microscope (30). AO stains DNA bright green, allowing visualization of the nuclear chromatin pattern.

Apoptotic cells have condensed chromatin, which is uniformly stained. EtBr stains DNA orange but is excluded by viable cells. AO and EtBr were each dissolved in PBS to a concentration of 100 μg/mL. Stock solutions (200 mmol/L in DMSO) were further diluted in PBS. The final concentration of DMSO was 0.05%, a level that had no effect on cell viability. The cells were seeded in 24-well plates and treated 24 h later. At the end of each experiment, the cells were trypsinized and pelleted together with the cells from the culture supernatant. After centrifugation at 400*g* at 37°C, the supernatant was removed and the cells were stained with 4 μL AO/EtBr solution (100 μg/mL AO in PBS:100 μg/mL EtBr in PBS = 1:1, v/v), mixed gently and examined under a fluorescence microscope using 40× magnification. At least 100 cells were counted and the percentage of affected cells was calculated. The cells were scored as alive if their nuclei displayed a normal morphology and were green. Cells with a normal morphology and an orange color were deemed to be necrotic. The cells were scored as apoptotic if their nuclei contained condensed chromatin and/or displayed nuclear fragmentation (29).

Measurement of Intracellular ATP

The cellular ATP content was determined with the ATP assay system bioluminescence detection kit (Calbiochem), according to the manufacturer's instructions. For reagent reconstitution, the ATP-monitoring enzyme was combined with 220 μL enzyme reconstitution buffer (1 μL per assay). Necrosis was induced in PC-12 cells by either KCN or STS/oligomycin-A, as described above. ATP measurements were done 1 h after induction of necrosis. At the end of the incubation period, the culture medium was removed and the cells were treated with 100 μL nucleotide-releasing buffer for 5 min at room temperature with gentle shaking. ATP-monitoring enzyme (1 μL) was added to the cell lysate. The ATP content of the sample was measured with the luciferin–luciferase method by using a luminometer. An ATP standard calibration curve was generated by using a series of ATP dilutions ranging from 0.001 to 1 mg/mL, from standard solution prepared by dissolving 1 mg ATP in 1 mL water.

Isolation of Rat Liver Mitochondria

Mitochondria were isolated from the livers of Sprague-Dawley female rats (200–300 g) by differential centrifugation as described previously (31,32). The livers were homogenized in ice-cold mitochondria isolation buffer (250 mmol/L sucrose, 0.1 mmol/L EDTA, 1 μg/mL leupeptine, 0.15 μmol/L phenylmethanesulfonyl fluoride and 10 mmol/L HEPES/KOH, pH = 7.2), 3 mL/mg liver, by using an electric homogenizer at 1,000 rpm for 10 min. The buffer volume was doubled and the homogenate was centrifuged at 1,000*g* for 5 min at 4°C. The pellet was homogenized again as described above and the supernatants were combined. The combined supernatant was centrifuged at 1,000*g* for 5 min at 4°C and the pellet was discarded. The supernatant was then centrifuged at 12,000*g* for 10 min at 4°C, and the pellet was resuspended in a fresh buffer at 8 mg/mL and centrifuged again at 12,000*g* for 10 min at 4°C. The pellet was then resuspended in a minimal volume in mitochondria isolation buffer without EDTA. Protein concentration was determined using the Biuret assay.

ATP Synthase Enzyme Activity Assay

ATP synthase activity was measured by using an ATP Synthase Enzyme Activity Microplate Assay Kit (Abcam), according to the manufacturer's protocol and published methods (33). Briefly, 10 μg ATP synthase (per well) were detergent-extracted from mitochondria lysates and immunocaptured for 3 h in 96-well plates. AGA(C8R)-HNG17 and controls were added to the immobilized enzyme and incubated for 45 min before the addition of the reagent mix and measurement. The decrease in absorbance as NADH is oxidized to NAD^+ was measured at 340 nm in a kinetic program. The experiments were performed three times, in duplicate.

Traumatic Brian Injury

The TBI model uses a weight-drop device that is designed to deliver a standard blow to the cranium, resulting in a controlled cerebral injury. The impact is delivered by a silicone-coated 5-mm metal tip extruding from a platform that falls down from a frame; this device was custom-made for this purpose. The impact imparted to the cranium of the mouse is proportional to the momentum of the 95-g platform at the end of its free fall (34). The neurobehavioral statuses of the mice were evaluated by using a set of 10 tasks that test reflexes, alertness, coordination and motor abilities. One point is awarded for failure to perform a particular task. The following parameters were measured: presence of monoparesis or hemiparesis, inability to walk on a 3-cm-wide beam, inability to walk on a 2-cm-wide beam, inability to walk on a 1-cm-wide beam, inability to balance on a round stick (0.5 cm wide), inability to balance on a 1-cm-wide beam, failure to exit a 30-cm-diameter circle (within 2 min), inability to walk straight, loss of startle behavior and loss of seeking behavior. Each mouse was awarded one point for every task it failed. Nine- to eleven-week-old C57BL/6J male mice were anesthetized by isoflurane and received moderate trauma to the brain (score of 4–6). The neuronal severity score (NSS) was determined 1 h after head injury (35), and, subsequently, histological tests were performed by MRI. The mice were then randomly sorted into groups and treated with AGA(C8R)-HNG17 in different doses or vehicle, which were injected into the intracerebral spine by direct puncture of the cisterna magna, 5 h after TBI delivery. Additional NSS tests and MRI scans were performed 1, 2 and 7 d after trauma to evaluate the long-term effect of the treatment. All animal experiments and handling protocols were approved by the Ben-Gurion University of the Negev Committee for the Ethical Care and Use of Animals in Research (permit number IL-10-03-2013).

Magnetic Resonance Imaging

MRI measurements were performed in a 1 tesla microMRI device (Aspect Imaging). Mice were under anesthesia (1–5% isofluorane in O_2) during the scan. T_2-weighted images of each mice's head were acquired every 0.9 microns, 18 slices total per mouse per scan. The edema was measured, since it differentiated from the healthy tissue by an increase in water efflux, which is depicted as brighter voxels. The edema volume was calculated as a percentage of the high brightness voxels from the total brain voxels by using a MATLAB algorithm for MRI measurements taken from the MATLAB central file exchange community.

Statistical Analysis

Each experiment was performed at least three times in duplicate. The data are presented as means ± standard error. Statistical analyses were performed with a Student *t* test. Significance was set at $P < 0.05$.

All supplementary materials are available online at www.molmed.org.

RESULTS

This study aimed to explore the antinecrotic functions of humanin and its derivatives. For this purpose, humanin and three of its derivatives (Table 1), previously shown to possess protective antiapoptotic effects against Alzheimer's disease (7–9,36), were first tested for their *in vitro* antinecrotic effects. The peptides were synthesized and purified in our laboratory, and their identity and purity were confirmed by MALDI-TOF MS and analytical HPLC (Supplementary Table S1). The peptides were first examined *in vitro* by using previously published models of necrosis (6,37). The first model for necrosis was chemohypoxia induced by cyanide (in the form of the potassium salt, KCN) in glucose-free medium (that is, conditions where apoptotic cell death is negligible) (37–39). In this model, ATP synthesis in the mitochondria is inhibited, since cyanide inactivates cytochrome-c oxidase; thus, cell death occurs by necrosis due to lack of sufficient ATP. Necrotic cell death in PC-12 cells was evaluated by measuring cell viability using trypan blue exclusion assay. AGA(C8R)-HNG17 (Table 1), which showed the highest activity against amyloid-β toxicity (15), was tested for its antinecrotic activity. AGA(C8R)-HNG17 exhibited a dose-dependent protective effect against KCN-induced cell death (Figure 1A), where 10 μmol/L AGA(C8R)-HNG17 increased cell viability from $(2.8 \pm 0.2) \times 10^5$ cells/mL to $(4.6 \pm 0.3) \times 10^5$ cells/mL. A significant effect was also observed with 1 μmol/L peptide concentration, where the half maximal inhibitory concentration (IC_{50}) was calculated to be 2.8 μmol/L.

Table 1. Amino acid sequences of humanin and its derivatives examined in the present study.

Peptide name	Amino acid sequence[a]
Humanin (HN)	MAPRGFSCLLLLTSEIDLPVKRRA
HNG	MAPRGFSCLLLLT**G**EIDLPVKRRA
AGA-HNG	MAP**A**G**A**SCLLLLT**G**EIDLPVKRRA
AGA(C8R)-HNG17	P**A**G**A**S**R**LLLLT**G**EIDLP

[a]Bold letters indicate humanin amino acid residues replaced in the derivatives. MS and analytical HPLC data of the peptides are given in Supplementary Table S1.

Another model of necrosis examined for these peptides is induction of cell death under conditions that shift apoptosis to necrotic cell death, through the addition of STS to cells in glucose-free medium, in the presence of oligomycin-A (an inhibitor of F_0F_1-ATPase) (26,27). Under these conditions, where ATP synthesis in the mitochondria is blocked, apoptosis, which requires ATP, cannot proceed—thus, cell death is shifted to necrosis (40). While taking into account the occurrence of apoptosis to a certain extent, scoring of necrotic cells was performed by staining with two different dyes—AO and EtBr—together with visualization of the nuclear morphology (see "Morphological Quantification of Necrosis and Apoptosis with Ethidium Bromide and Acridine Orange" in the experimental section). Figure 1B shows the percentage of necrotic-scored PC-12 cells upon exposure to STS and oligomycin-A toxicity, and their treatment by humanin and its derivatives is listed in Table 1. As can be seen in Figure 1B, addition of oligomycin-A or STS alone did not induce significant necrosis, whereas oligomycin-A and STS together induced 59% necrosis, as measured by AO/EtBr double staining. Pretreatment of cells with 10 μmol/L humanin or its derivatives reduced the necrotic cell death from 59% to 38% to 42% (depending on the peptide used; Figure 1B). The protective effects of 10 μmol/L humanin or its derivatives in the STS and oligomycin-A model for necrosis were also evaluated by measuring cell death by lactate dehydrogenase release. Pretreatment of PC-12 cells by humanin derivatives reduced lactate dehydrogenase released under STS and oligomycin-A toxicity from 49% of vehicle treatment to 26–28% (Figure 1C). The lactate dehydrogenase assay showed higher levels of protection afforded by the peptides than for the AO/EtBr assay, which may be attributable to the disruptive impacts of the AO/EtBr assay, which in turn could have affected the counting of stained cells.

The protective effects of humanin and its derivatives in the KCN model for necrosis were further examined in the NSC-34 cell line of neuromuscular origin, as measured by the lactate dehydrogenase release assay (Figure 1D). All tested peptides conferred protection from necrotic cell death, with AGA-HNG presenting the best protection by reducing lactate dehydrogenase release from 46 ± 7% to 19 ± 3%.

In summary, the protective effects of humanin and its derivatives against necrotic cell death were observed in both PC-12 and NSC-34 cells. Among the pep-

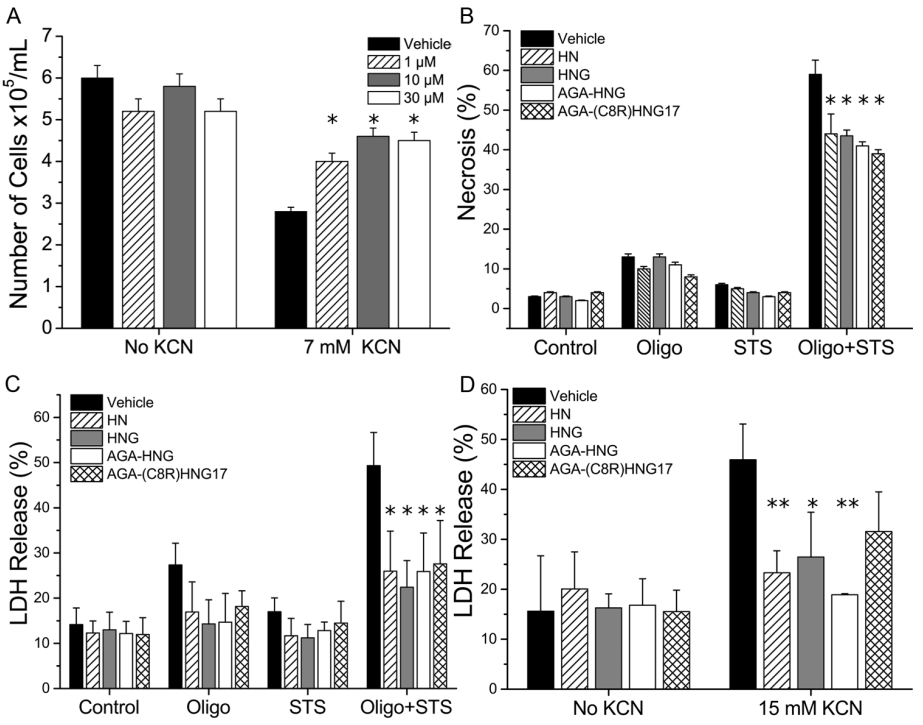

Figure 1. Humanin and its derivatives inhibit necrosis in neuronal cells *in vitro*. (A) Dose-dependent protective effect of AGA(C8R)-HNG17 on the viability of PC-12 cells treated with KCN, as assessed by trypan blue exclusion. **P* ≤ 0.04 (*t* test), as compared with vehicle with KCN; n = 3. (B) The antinecrotic effect of 10 μmol/L humanin and its derivatives in PC-12 cells under necrotic conditions induced by STS/oligomycin-A (Oligo + STS), as assessed by AO/EtBr double staining. The protective effect against oligomycin-A (Oligo) and STS alone is also shown. **P* ≤ 0.05 (*t* test), as compared with vehicle; n = 3. (C) The antinecrotic effect of 10 μmol/L humanin and its derivatives in the same experimental setup as in (B), with lactate dehydrogenase (LDH) release reflecting cell death. **P* ≤ 0.04 (*t* test), as compared with vehicle; n = 3. (D) LDH release in NSC-34 cells under necrotic conditions induced by 15 mmol/L KCN with or without treatment with 10 μmol/L humanin peptides. **P* ≤ 0.02 and ***P* ≤ 0.05 (*t* test) compared with vehicle treatment with KCN; n = 3.

tides tested, AGA(C8R)-HNG17 showed the highest inhibition potency in the STS and oligomycin-A model and in the chemohypoxia by KCN in PC-12 cells (Figures 1A–C), whereas AGA-HNG was the most potent peptide in the KCN model for NSC-34 cells (Figure 1D).

Based on the *in vitro* results, we next extended our study to include the *in vivo* model of necrosis-related diseases. Peptide-protective activities were evaluated by using mice to model TBI (34,41), where necrosis is a major cell death pathway under moderate trauma conditions (42). The TBI model uses a weight-drop device that is designed to deliver a standard blow to the cranium, resulting in a controlled cerebral injury. The resultant brain injury and recovery from it were monitored 1 h and 1, 2 and 7 d after TBI by both neurobehavioral assessment and histological measurement (35) (see Figure 2A for experimental design and Figure 2B for representative MRI scans). The mice were randomly sorted into groups 5 h after TBI delivery, and then AGA(C8R)-HNG17 (Table 1) was administered by intracerebral spinal injection. AGA(C8R)-HNG17 was selected for *in vivo* studies because of its pronounced activity *in vitro* (Figure 1).

As previously noted, neurobehavioral status of the mice was assessed by assigning an NSS, after testing mouse reflexes, alertness, coordination and motor abilities (see "Traumatic Brain Injury" in the experimental section). The NSS of mice 1 h after a TBI was 4.5 ± 0.6 points (Figure 2C), and the average score of vehicle-treated mice 24 h after TBI delivery was 1.6 ± 0.5 points. Mice treated with 0.04 and 1.2 mg/kg of AGA(C8R)-HNG17 had an average score of 1.0 ± 0.5 points. However, mice treated with 0.4 mg/kg AGA(C8R)-HNG17 had an average NSS score of 0.6 ± 0.5 points, which significantly differs from the vehicle-treated group (Figure 2C). At 48 h after TBI and onwards, the NSS values of all the groups were similar, and no significant differences between the score of each group were measured: 0.5 ± 0.5 and 0.3 ± 0.5 points after 48 h and 7 d, respectively.

Histological measurements of the brain edema volume of the mice were performed by measuring T_2 relaxation by small-animal MRI (microMRI) 1 h, 1 d, 2 d and 7 d after TBI, following the NSS grading (see Figure 2A for experimental design). The edema were measured by using an MRI, and their volume was calculated as a percentage of the total brain volume. The first measurement was done 1 h after TBI induction, and the average edema volume was 12 ± 4 % of the brain volume (Figure 2D); the mice were then randomly sorted into groups. Recovery follow-up started 24 h after TBI (Figure 2D). While the average edema volume of vehicle-treated mice and the mice treated with 0.04 mg/kg peptide was not significantly different (13 ± 4 and 11 ± 4% of the brain, respectively), the average edema volume of mice treated with 0.4 mg/kg peptide was considerably lower (8 ± 2 % of the brain volume). After 48 h from TBI delivery, the edema volume of the vehicle-treated mice was 11 ± 2%; for mice treated with 0.04 mg/kg peptide, it was 9 ± 4%; and the edema volume of mice treated with 0.4 mg/kg was 7 ± 2%. A week after trauma induction, the MRI analyses showed a continued reduction in edema volume in all mice groups. Whereas vehicle-treated mice had an edema volume of 7 ± 1%, all AGA(C8R)-HNG17 treated

mice had a slightly smaller edema volume of 5 ± 2%. Of note, a higher dose (1.2 mg/kg) of AGA(C8R)-HNG17 was tested, resulting in a similarly protective effect (data not shown).

The histological measurements showed that 0.4 mg/kg peptide was the optimal dose for neuronal protection, which is in agreement with the neuronal severity score tests (Figure 2C). Hence, AGA(C8R)-HNG17 can protect mice against cell death when it is administered 5 h after moderate TBI, where necrosis is the predominant mechanism of cellular destruction (42).

It was previously demonstrated that depletion of cellular ATP levels predisposes cells to necrotic death (26,43,44). Previous studies have shown that humanin can increase ATP levels in different cell types, such as human lymphocytes, TE671 muscle cells and neural SKN-MC cells (25). It was therefore important to determine whether or not the antinecrotic activity of AGA(C8R)-HNG17, which was observed in the necrosis experimental system in this study, was mediated via elevation of intracellular ATP levels. ATP levels were measured in PC-12 cells undergoing necrosis induced by chemohypoxia with KCN or by STS/oligomycin-A and pretreated by AGA(C8R)-HNG17 at different concentrations (Figure 3A). Under necrotic conditions induced by chemohypoxia, ATP levels decreased from 4.9 ± 0.2 fmole/cell to 2.5 ± 0.2 fmole/cell; AGA(C8R)-HNG17 at 10 μmol/L elevated intracellular ATP levels to 4.2 ± 0.2 fmole/cell (Figure 3A). Under necrotic conditions induced by STS/oligomycin-A, AGA(C8R)-HNG17 showed even more pronounced effects, where 1 μmol/L peptide elevated ATP levels from 2.0 ± 0.2 fmole/cell to 4.9 ± 0.3 fmole/cell (Figure 3A).

In the necrosis models used in this study, mitochondrial ATP synthesis was blocked by either KCN or oligomycin-A. As ATP synthase is the main source of mitochondrial ATP production, we next examined whether AGA(C8R)-HNG17 has a direct effect on the enzyme. We

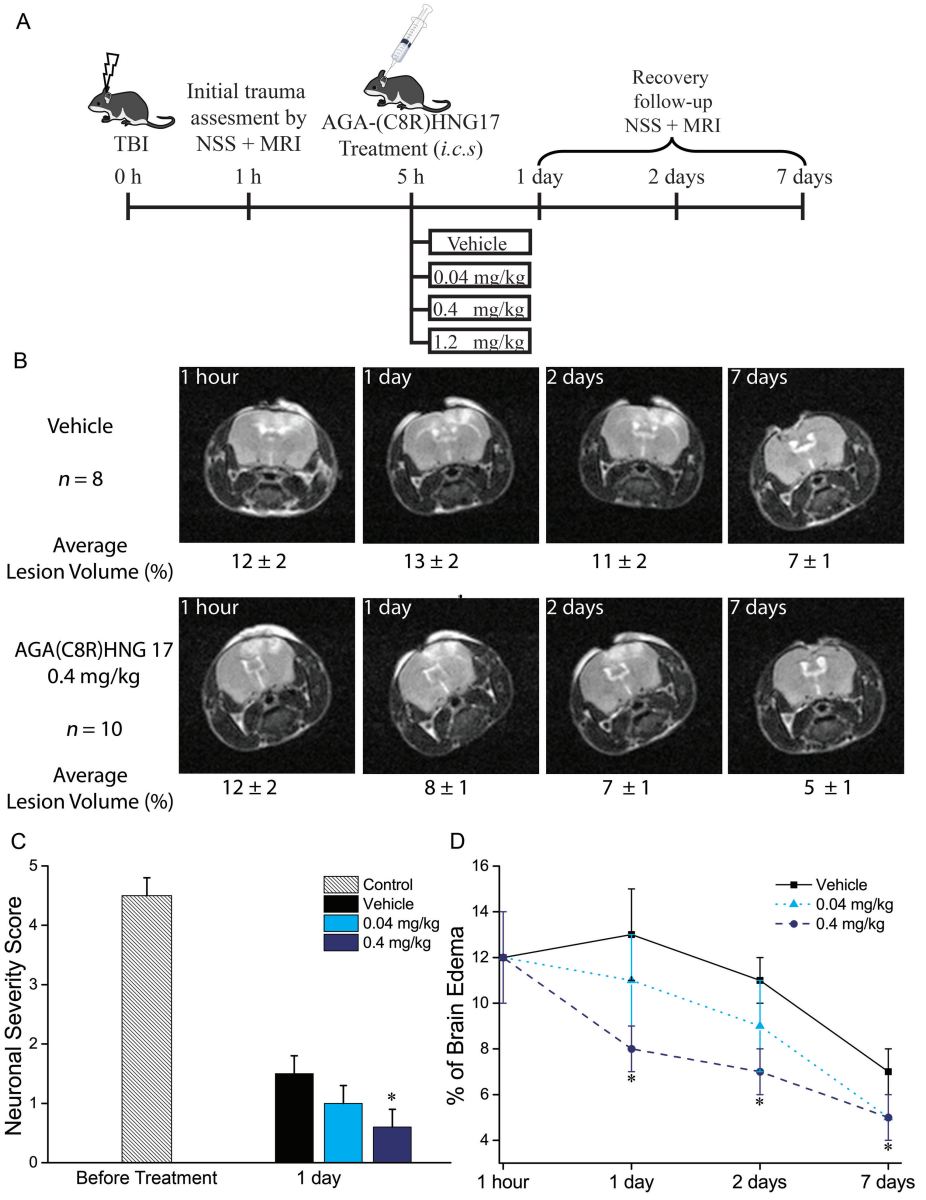

Figure 2. The protective effect of AGA(C8R)-HNG17 in mice against TBI. (A) Experimental design for the data obtained *in vivo*. (B) MRI scans of representative mice brains: median mouse from each group with the group average values given below each image ± standard deviation. (C) Neuronal severity score for groups of mice treated with vehicle (n = 8), 0.04 mg/kg (n = 8) or 0.4 mg/kg (n = 10) of AGA(C8R)-HNG17, tested 1 and 24 h after TBI. *$P \leq 0.002$ (*t* test) compared with vehicle measurement on the same time point. (D) Graph showing the average values of brain edema for the groups of mice treated with different concentrations of AGA(C8R)-HNG17 (n = 8 for 0.04 and n = 10 for 0.4 mg/kg) or vehicle (n = 8) as a percent of the brain volume. MRI scans were performed 1 h and 1, 2 and 7 d after TBI. *$P \leq 0.05$ (*t* test) compared with the respected time-point vehicle group value.

thus tested the effect of the peptide on the activity of ATP synthase isolated from rat liver mitochondria. ATP synthase activity was measured by following the decrease in NADH levels spectrophotometrically during its oxidation to NAD^+. The results show dose-dependent activity for AGA(C8R)-

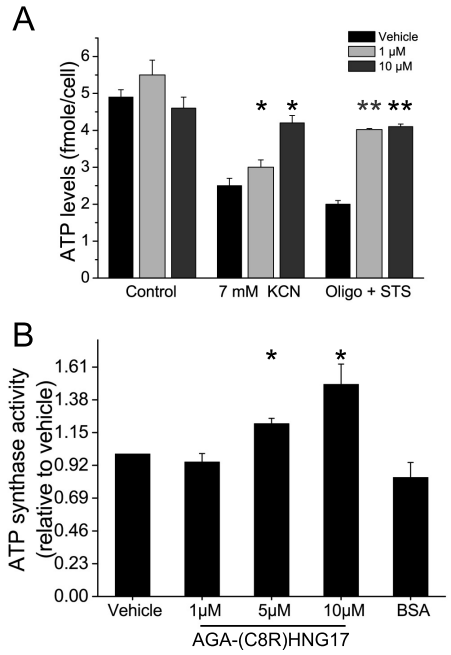

Figure 3. The effect of AGA(C8R)-HNG17 on intracellular ATP production. (A) Intracellular ATP levels of PC-12 cells treated with different concentrations of AGA(C8R)-HNG17 under necrotic conditions induced by chemohypoxia with KCN or by STS/oligomycin-A. ATP levels were detected by measuring bioluminescence in cells extracts via the luciferin–luciferase method. *$P \leq 0.05$ (*t* test) compared with treatment with KCN with vehicle; n = 3; **$P \leq 0.05$ (*t* test) compared with treatment with oligomycin-A and STS with vehicle; n = 3. (B) The effect of different concentrations of AGA(C8R)-HNG17 on the activity of ATP synthase (relative to vehicle) isolated from rat liver mitochondria, measured by following the decrease in NADH absorbance at 340 nm. The average rate of decrease in NADH absorbance of the control was 0.97 ± 0.06 mAU/min. *$P \leq 0.005$ (*t* test) compared with vehicle, n = 3.

HNG17, where 10 μmol/L peptide induced a 49.0 ± 0.3% increase in ATP synthase activity over the vehicle (Figure 3B). A control of 17 mg/L BSA, which is analogous to the weight concentration of AGA(C8R)-HNG17, did not show any effect on the enzymatic activity. The direct effect of AGA(C8R)-HNG17 on ATP synthase activity implies that the antinecrotic activities of AGA(C8R)-HNG17 were mediated through elevation of intracellular ATP levels by mitochondrial ATP synthase.

DISCUSSION

It was previously shown that humanin has antiapoptotic activity against amyloid β toxicity, and it has been forwarded as a potential neuroprotective agent in treating Alzheimer's disease and amyotrophic lateral sclerosis (ALS) (16,45,46). In this study, we show for the first time that humanin derivatives exhibit neuroprotective effects in experimental models for necrotic cell death *in vitro* and *in vivo*. Our study reveals that AGA(C8R)-HNG17 confers protection to cells at risk of necrotic cell death. The inhibition of necrosis by the humanin derivative was assessed in PC-12 and NSC-34 cells, by using two different inducers for necrosis (KCN and STS/oligomycin-A) under glucose-depleting conditions previously shown to instantiate necrotic cell death, as opposed to apoptosis (26,27,40). These models for necrosis were optimized in our lab before studying the inhibitory effects of the humanin peptides (6,37). The experimental system was designed in a way that allows necrosis inhibitors to affect the necrotic process before the irreversible phase of cellular membrane disintegration. Necrotic cell death was confirmed by both morphological analysis (AO/EtBr double staining) and lactate dehydrogenase release. The AGA(C8R)-HNG17 and AGA-HNG peptides were the most effective derivatives in protecting PC-12 and NSC-34 cells from necrosis, which is consistent with their reported high antiapoptotic activity (15). The peptides' *in vitro* antinecrotic activities discovered in this study were at the low micromolar range, with AGA(C8R)-HNG17 IC_{50} of 2.8 μmol/L in PC-12 cells. This activity was independent of the necrosis inducers and was not cell line specific. The IC_{50} value for protection against necrosis was found to be higher than the reported IC_{50} value for protection against apoptosis. This difference can be attributed to different cellular mechanisms and targets that are involved in protection against necrosis compared with apoptosis; the two pathways involve different signaling mechanisms.

On the basis of the results obtained *in vitro*, the next step was to assess the protective activity of AGA(C8R)-HNG17 against necrotic cell death *in vivo*, by using moderate TBI as a model (34,41). In moderate TBI, necrosis was shown to be the predominant mechanism of cellular destruction (42). The initial blow causes an irreversible damage to brain cells near the impact site, which results in secondary necrotic damage to the surrounding tissue. Thus, it was necessary to follow the recovery during short-time periods (1–2 d) and validate the success of the treatment after a longer duration (7 d). Indeed, histological measurements of mice brain tissue showed a decrease in damaged area for animals treated with AGA(C8R)-HNG17 (Figures 2B, D). Dose-response analyses of the peptide effect on brain edema were in agreement with the neuronal severity score tests, where 0.4 mg/kg peptide was the optimal dose for neuronal protection of the brain (Figures 2C, D).

These neuro-protective activities against necrosis were already in play from the beginning; no additional injections were needed. Hence, the results indicate that AGA(C8R)-HNG17 can protect brain tissue from secondary necrosis resulting from TBI.

Significantly, the effect of the trauma on necrosis reaches a maximum within a few hours post-trauma, and thereafter a gradual recovery begins. Indeed, there is a decrease in the edema volume and in the NSS, already apparent in the vehicle group along time. This is known to be attributable to natural recovery supported by neighboring cells that compensate for damaged cells, and this has also been observed in previous studies that use this model (35,41). This transient nature of necrosis induced by trauma *in vivo*, as observed in Figure 2D, explains why the protective effect of AGA(C8R)-HNG17 is seen mainly after 1 d. This timeframe is known to be critical for treatment of trauma—whereas other intrinsic factors

are active *in vivo* in brain recovery after longer periods. Humanin derivatives' protective effects exhibited *in vivo* are in agreement with the protective effects observed *in vitro*. However, because of the complexity of the brain tissue/*in vivo* model, differences in kinetics of necrosis inhibition may be observed.

Previous publications have highlighted the protective effects of humanin peptides in a brain ischemia reperfusion model for stroke, by using middle cerebral artery occlusion (13). In this model, the main pathway of cellular demise occurs via a caspase-mediated pathway and not via classical necrosis (47). Here, for the first time, to the best of our knowledge, we show that humanin, as much as possible, moves to minimize secondary necrosis associated with TBI. This study thus expands our knowledge of the activities of humanin, adding antinecrotic properties to its known antiapoptotic effects.

An important insight into the mechanism was attained by measuring ATP levels in PC-12 cells, which underwent necrosis by either KCN or STS/oligomycin-A, where AGA(C8R)-HNG17 was found to elevate intracellular ATP levels in a dose-dependent manner (Figure 3A). These results are consistent with previous studies performed with human lymphocytes, muscle cells and neurons showing that humanin peptides, used at concentrations similar to those seen here, elevated cellular ATP levels (25,48). Moreover, this is the first time that humanin peptides have been shown to increase ATP levels under necrotic conditions. Hence, it is suggested that the inhibition of necrosis by AGA(C8R)-HNG17 was achieved via elevation of intracellular ATP levels.

ATP synthase is located along the mitochondrial inner membrane and is the main producer of mitochondrial ATP. AGA(C8R)-HNG17 was found to enhance the activity of ATP synthase by ~50%, isolated from rat liver mitochondria (Figure 3B). To the best of our knowledge, this is the first report identifying a direct effect of a humanin peptide on ATP synthase activity. The enhancement of ATP synthase activity by AGA(C8R)-HNG17 implies that the antinecrotic actions of this peptide were mediated through elevation of intracellular ATP levels and thus could be beneficial under stress conditions such as necrosis.

Multiple mechanisms were suggested to explain the antiapoptotic modes of action of humanin, including activation of the transcription factor STAT3 by phosphatidylinositol (PI) 3-kinase/Akt, as well as inactivation of BAX (18,21–23). However, mitochondrial ATP production and the fast kinetics of signal transduction in necrotic cell death rule out the involvement of transcription factors (6,49). Moreover, BAX was shown to be a proapoptotic protein rather than mediating necrosis (50).

The results presented in this study imply that the peptide's modes of action were related to mitochondrial processes because of the following: (a) elevation of cellular ATP levels by AGA(C8R)-HNG17 takes place under the conditions of a glucose-free medium, which was fortified by the mitochondrial energy substrate pyruvate, ruling out glycolytic contribution to ATP synthesis; (b) the fact that the necrosis-inducers KCN and oligomycin-A directly target the mitochondrial electron transport chain, which is responsible for mitochondrial ATP production; and (c) the ability of AGA(C8R)-HNG17 to increase the rate of isolated mitochondrial ATP synthase activity. The effect of humanin on ATP levels by itself does not exclude the possibility of involvement of other mechanisms in which humanin protects against necrotic cell death.

That mitochondria is the target for the protective effects of the humanin derivative is further supported by a previous work that demonstrates that HNG protects PC-12 cells from mitochondria dysfunction by preserving mitochondrial membrane potential, thus conferring protection against amyloid β toxicity (51). Although the mechanistic basis of peptide-mediated protection against necrosis merits further investigation, the results of the present study imply that AGA(C8R)-HNG17 targets the mitochondria. It is thus possible that increasing ATP levels is an important contribution for protection against the impending necrotic process.

CONCLUSION

The present study shows that the humanin-derivative AGA(C8R)-HNG17 has antinecrotic effects, which suggests it has a potential use as a lead compound for developing new treatments for necrosis-associated diseases. This novel function of humanin adds to its already-known antiapoptotic activity, making humanin a potential agent to combat conditions in which both necrosis and apoptosis are involved. More specifically, the humanin derivative may lead to the development of novel therapeutic interventions to combat ischemic states such as stroke, TBI and myocardial infraction, conditions for which no efficient drug-based treatment is currently available.

ACKNOWLEDGMENTS

The authors thank Mark M Karpasas and Lina Saveliev from the Analytical Research Services Unit, Ben-Gurion University of the Negev, for mass spectrometric analysis of the peptides, and Svetlana Lublinsky from the Brain Imaging Center, Ben-Gurion University of the Negev, for magnetic resonance imaging of the mice. The financial support of the Kamin Program from the Chief Scientist of the Ministry of Economy of Israel (to AH Parola, I Nathan, and R Kasher), the James-Frank Center for Laser-Matter Interaction (to A H Parola), the Edmund Safra Foundation for Functional Bio-polymer, the New-York University Shanghai (NYUSH) research grant (to AH Parola) and the Lyonel Israels' Chair Fund (I Nathan) are gratefully acknowledged.

DISCLOSURE

The authors declare that they have no competing interests as defined by *Molecular Medicine*, or other interests that might be perceived to influence the results and discussion reported in this paper.

REFERENCES

1. Alison MR, Sarraf CE. (1994) Liver cell death: patterns and mechanisms. *Gut*. 35:577–81.
2. Zhivotovsky B, Orrenius S. (2010) Cell death mechanisms: cross-talk and role in disease. *Exp. Cell Res.* 316:1374–83.
3. Saikumar P, Dong Z, Weinberg JM, Venkatachalam MA. (1998) Mechanisms of cell death in hypoxia/reoxygenation injury. *Oncogene.* 17:3341–9.
4. Shi Y. (2001) A structural view of mitochondria-mediated apoptosis. *Nat. Struct. Biol.* 8:394–401.
5. Moquin D, Chan FK-M. (2010) The molecular regulation of programmed necrotic cell injury. *Trends Biochem. Sci.* 35:434–41.
6. Tsesin N, Khalfin B, Nathan I, Parola AH. (2014) Cardiolipin plays a role in KCN-induced necrosis. *Chem. Physics Lipids*.183:159–68.
7. Hashimoto Y, *et al.* (2001) A rescue factor abolishing neuronal cell death by a wide spectrum of familial Alzheimer's disease genes and Abeta. Proc Natl Acad Sci USA 98:6336–6341.
8. Hashimoto Y, *et al.* (2001) Mechanisms of neuroprotection by a novel rescue factor humanin from Swedish mutant amyloid precursor protein. *Biochem. Biophys. Res. Commun.* 283:460–468.
9. Hashimoto Y, *et al.* (2001) Detailed characterization of neuroprotection by a rescue factor humanin against various Alzheimer's disease-relevant insults. *J. Neurosci.* 21:9235–9245.
10. Muzumdar RH, *et al.* (2009) Humanin: A Novel Central Regulator of Peripheral Insulin Action. PLoS One 4: e6334.
11. Sponne I, *et al.* (2004) Humanin rescues cortical neurons from prion-peptide-induced apoptosis. *Mol. Cell. Neurosci.* 25:95–102.
12. Kariya S, *et al.* (2002) Humanin inhibits cell death of serum-deprived PC12h cells. *Neuroreport.* 13:903–7.
13. Xu X, Chua CC, Gao J, Hamdy RC, Chua BH. (2006) Humanin is a novel neuroprotective agent against stroke. *Stroke.* 37:2613–9.
14. Terashita K, *et al.* (2003) Two serine residues distinctly regulate the rescue function of Humanin, an inhibiting factor of Alzheimer's disease-related neurotoxicity: functional potentiation by isomerization and dimerization. *J. Neurochem.* 85:1521–38.
15. Chiba T, *et al.* (2005) Development of a femtomolar-acting humanin derivative named colivelin by attaching activity-dependent neurotrophic factor to its N terminus: characterization of colivelin-mediated neuroprotection against Alzheimer's disease-relevant insults in vitro and in vivo. *J. Neurosci.* 25:10252–61.
16. Ying G, *et al.* (2004) Humanin, a newly identified neuroprotective factor, uses the G protein-coupled formylpeptide receptor-like-1 as a functional receptor. *J. Immunol.* 172:7078–85.
17. Harada M, *et al.* (2004) N-Formylated humanin activates both formyl peptide receptor-like 1 and 2. *Biochem. Biophys. Res. Commun.* 324:255–61.
18. Hashimoto Y, *et al.* (2005) Involvement of tyrosine kinases and STAT3 in humanin-mediated neuroprotection. *Life Sci.* 77:3092–104.
19. Matsuoka M, Hashimoto Y. (2010) Humanin and the receptors for humanin. *Mol. Neurobiol.* 41:22–8.
20. Hashimoto Y, Kurita M, Aiso S, Nishimoto I, Matsuoka M. (2009) Humanin inhibits neuronal cell death by interacting with a cytokine receptor complex or complexes involving CNTF receptor alpha/WSX-1/gp130. *Mol. Biol. Cell.* 20:2864–73.
21. Guo B, *et al.* (2003) Humanin peptide suppresses apoptosis by interfering with Bax activation. *Nature.* 423:456–61.
22. Zhai D, *et al.* (2005) Humanin binds and nullifies Bid activity by blocking its activation of Bax and Bak. *J. Biol. Chem.* 280:15815–24.
23. Luciano F, *et al.* (2005) Cytoprotective peptide humanin binds and inhibits proapoptotic Bcl-2/Bax family protein BimEL. *J. Biol. Chem.* 280:15825–35.
24. Niikura T, Chiba T, Aiso S, Matsuoka M, Nishimoto I. (2004) Humanin: after the discovery. *Mol. Neurobiol.* 30:327–40.
25. Kariya S, Hirano M, Furiya Y, Ueno S. (2005) Effect of humanin on decreased ATP levels of human lymphocytes harboring A3243G mutant mitochondrial DNA. *Neuropeptides.* 39:97–101.
26. Leist M, Single B, Castoldi AF, Kuhnle S, Nicotera P. (1997) Intracellular adenosine triphosphate (ATP) concentration: a switch in the decision between apoptosis and necrosis. *J. Exp. Med.* 185:1481–6.
27. Eguchi Y, Shimizu S, Tsujimoto Y. (1997) Intracellular ATP levels determine cell death fate by apoptosis or necrosis. *Cancer Res.* 57:1835–40.
28. Strober W. (2001) Trypan blue exclusion test of cell viability. *Curr. Protoc. Immunol.* (Suppl 21 Appx 3B):A.3B.1–A.3B.2.
29. Shapira MG, Khalfin B, Lewis EC, Parola AH, Nathan I. (2014) Regulation of autophagy by α(1)-antitrypsin: "A foe of a foe is a friend." *Mol. Med.* 20:417–26.
30. Hallak M, *et al.* (2009) The anti-leukaemic activity of novel synthetic naphthoquinones against acute myeloid leukaemia: induction of cell death via the triggering of multiple signalling pathways. *Br. J. Haematol.* 147:459–70.
31. Hallak M, *et al.* (2008) A molecular mechanism for mimosine-induced apoptosis involving oxidative stress and mitochondrial activation. *Apoptosis.* 13:147–55.
32. Zalk R, Israelson A, Garty ES, Azoulay-Zohar H, Shoshan-Barmatz V. (2005) Oligomeric states of the voltage-dependent anion channel and cytochrome c release from mitochondria. *Biochem. J.* 386:73–83.
33. Alavian KN, *et al.* (2011) Bcl-xL regulates metabolic efficiency of neurons through interaction with the mitochondrial F1FO ATP synthase. *Nat. Cell Biol.* 13:1224–33.
34. Feldman Z, *et al.* (1996) Effect of magnesium given 1 hour after head trauma on brain edema and neurological outcome. *J. Neurosurg.* 85:131–7.
35. Beni-Adani L, *et al.* (2001) A peptide derived from activity-dependent neuroprotective protein (ADNP) ameliorates injury response in closed head injury in mice. *J. Pharmacol. Exp. Ther.* 296:57–63.
36. Arakawa T, Kita Y, Niikura T. (2008) A rescue factor for Alzheimer's diseases: discovery, activity, structure, and mechanism. *Curr. Med. Chem.* 15:2086–98.
37. Zelig U, Kapelushnik J, Moreh R, Mordechai S, Nathan I. (2009) Diagnosis of cell death by means of infrared spectroscopy. *Biophys. J.* 97:2107–14.
38. Prabhakaran K, Li L, Borowitz JL, Isom GE. (2002) Cyanide induces different modes of death in cortical and mesencephalon cells. *J. Pharmacol. Exp. Ther.* 303:510–9.
39. Li L, Prabhakaran K, Mills EM, Borowitz JL, Isom GE. (2005) Enhancement of cyanide-induced mitochondrial dysfunction and cortical cell necrosis by uncoupling protein-2. *Toxicol. Sci.* 86:116–24.
40. Shchepina LA, *et al.* (2002) Oligomycin, inhibitor of the F0 part of H+-ATP-synthase, suppresses the TNF-induced apoptosis. *Oncogene.* 21:8149–57.
41. Cohen-Yeshurun A, *et al.* (2011) N-arachidonoyl-L-serine is neuroprotective after traumatic brain injury by reducing apoptosis. *J. Cereb. Blood Flow Metab.* 31:1768–77.
42. Raghupathi R. (2004) Cell death mechanisms following traumatic brain injury. *Brain Pathology.* 14:215–22.
43. Nicotera P, Leist M, Ferrando-May E. (1998) Intracellular ATP, a switch in the decision between apoptosis and necrosis. *Toxicol. Lett.* 102–103:139–42.
44. Prabhakaran K, Sampson DA, Hoehner JC. (2004) Neuroblastoma survival and death: an in vitro model of hypoxia and metabolic stress. *J. Surg. Res.* 116:288–96.
45. Chiba T, *et al.* (2006) Colivelin prolongs survival of an ALS model mouse. *Biochem. Biophys. Res. Commun.* 343:793–8.
46. Matsuoka M, Hashimoto Y, Aiso S, Nishimoto I. (2006) Humanin and colivelin: neuronal-death-suppressing peptides for Alzheimer's disease and amyotrophic lateral sclerosis. *CNS Drug Rev.* 12:113–22.
47. Puyal J, Ginet V, Clarke PGH. (2013) Multiple interacting cell death mechanisms in the mediation of excitotoxicity and ischemic brain damage: a challenge for neuroprotection. *Prog. Neurobiol.* 105:24–48.
48. Kariya S, Hirano M, Furiya Y, Sugie K, Ueno S. (2005) Humanin detected in skeletal muscles of MELAS patients: a possible new therapeutic agent. *Acta. Neuropath.* 109:367–72.
49. Hoang PT, *et al.* (2010) The neurosurvival factor Humanin inhibits β-cell apoptosis via signal transducer and activator of transcription 3 activation and delays and ameliorates diabetes in nonobese diabetic mice. *Metabolism.* 59:343–9.
50. Dewson G, Kluck RM. (2009) Mechanisms by which Bak and Bax permeabilise mitochondria during apoptosis. *J. Cell Sci.* 122:2801–8.
51. Jin H, *et al.* (2010) Protective effects of [Gly14]-Humanin on beta-amyloid-induced PC12 cell death by preventing mitochondrial dysfunction. *Neurochem. Int.* 56:417–23.

Cite this article as: Cohen A, *et al.* (2015) Humanin derivatives inhibit necrotic cell death in neurons. *Mol. Med.* 21:505–14.